Effect of molecular complexity on entropy mechanisms over shock waves

Stefan Cox

Technische Universiteit Delft, Delft, South Holland, 2628 CB, Netherlands

Supervised by:

Dr. Matteo Pini, Delft University of Technology
Dr. Andrea Spinelli, Polytechnic University of Milan

Understanding the inner workings of shock waves may unlock more precise tools for optimization of the design of rotating machinery and analysis of natural phenomena involving exotic, rapidly moving fluids, such as the formation of stars. This paper analyzes the mechanisms behind entropy generation and shock thickness over shock waves in different fluids though the numerical integration of one-dimensional fluid flow equations. It was determined that the proportion of entropy generated due to thermal conductivity increases with upstream Mach number and decreases with molecular complexity. Shock thickness decreases with molecular complexity and Mach number, due to the shortened mean free path and higher shock intensity, respectively. It is recommended to expand this method to enable the analysis of non-ideal fluids by introducing more precise equations of state, and to apply the findings of this research to the design of rotating machinery to minimize their fluid-dynamic loss over shock waves. [a]

Nomenclature

Greek Symbols

α	Dimensionless shock strength property	–
$\bar{\lambda}$	Dimensionless thermal conductivity	–
$\bar{\mu}$	Dimensionless viscosity	–
δ	Dimensionless fluid complexity property	–
η	Pressure ratio	–
γ	Ratio of specific heats	–
λ	Thermal conductivity	$\mathrm{W \cdot m^{-1} \cdot K^{-1}}$
μ	Combined viscosity	$\mathrm{Pa \cdot s}$
μ_1	Shear viscosity	$\mathrm{Pa \cdot s}$
μ_2	Compression viscosity	$\mathrm{Pa \cdot s}$
ω	Dimensionless velocity	–
ϕ	Dimensionless pressure	–
ρ	Density	$\mathrm{kg \cdot m^{-3}}$
τ	Viscous stress	Pa
θ	Dimensionless temperature	–
ζ	Nondimensional eigenvalue	–

Latin Symbols

$\dot{m}$	Area specific mass flow	$\mathrm{kg \cdot m^{-2} \cdot s^{-1}}$
ℓ_{mfp}	Mean free path	m
c_p	Mass specific constant pressure heat capacity	$\mathrm{J \cdot kg^{-1} \cdot K^{-1}}$
c_v	Mass specific constant volume heat capacity	$\mathrm{J \cdot kg^{-1} \cdot K^{-1}}$
E	Area specific energy	$\mathrm{kg \cdot s^{-3}}$
e	Specific internal energy	J/kg
$L(\omega, \theta)$	Dimensionless temperature gradient function	–
M	Mach number	–
$M(\omega, \theta)$	Dimensionless velocity gradient function	–
P	Area specific momentum	Pa
p	Pressure	Pa
q	Heat flux	$\mathrm{W \cdot m^{-2}}$
R	Specific gas constant	$\mathrm{J \cdot kg^{-1} \cdot K^{-1}}$
s	Entropy	$\mathrm{J \cdot kg^{-1} \cdot K^{-1}}$
T	Temperature	K
t	Shock thickness	m
t_{mfp}	Dimensionless shock thickness	–
u	Velocity	$\mathrm{m \cdot s^{-1}}$
x	Position	m
Z	Dimensionless coordinate of velocity and temperature	$(-, -)$

[a] Word count: 4376

Statement on the use of generative AI:
Generative AI was not used to generate this text.

I. Introduction

As the global demand for energy continues to increase, it becomes more critical to investigate alternate forms of clean energy production. One such underutilized method is the harvesting of waste heat from industrial processes, in which energy which would otherwise be dissipated into the atmosphere is re-purposed to produce electricity - all without emitting additional greenhouse gas. Harvesting thermal energy from industrial processes in the EU alone is estimated to be able to provide about 150 TWh of electricity, enough to meet the combined electricity demands of the Netherlands and Denmark [1].

The process in which unused energy is converted to electricity is based on the same principle used for steam power plants: the Rankine Cycle. Due to the wide range of temperatures exhibited in thermal waste producing industrial elements, water is often not a valid candidate as a working fluid for such applications. Organic molecules such as hydrocarbons, refrigerants, siloxanes or carbon dioxide, or mixes thereof are instead used as the working fluid. Whereas water is best applicable for turbines with high temperature and power output, turbines utilizing organic fluids efficiently generate electricity at low or medium temperature levels (as low as 100°C) and smaller power capacities (from a few kW to tens of MW) [1].

Although well-established methods are commonly used for the development of turbines which utilize steam or combustion gases, these do not translate to Organic Rankine Cycle (ORC) turbines, as they would produce incorrect sizing and performance estimations due to the difference in working fluid [2]. With this in mind, the properties of the ORC working fluids must be better understood in order to produce efficient designs.

Due to the nature of ORC turbines and their fluids, the thermodynamic properties of the fluid is often not accurately described by the ideal gas law. Additionally, the high molecular complexity causes low speeds of sound, creating transonic or supersonic flows within the turbine. Understanding the effects of these properties is key in properly designing ORC turbines.

One behavior which is critical in designing efficient turbines is the effect of shock waves on the fluid. The irreversible conversion of mechanical energy to internal energy over a shock wave is crucial in understanding a shock waves effect on a turbine. Creating an accurate simplified model of this allows for a prediction of the expected loss due to shock waves within the turbine without the need for expensive computational fluid dynamics programs or experiments, which expedites and simplifies the design process. Understanding the inner mechanisms of shockwaves also enables analysis of other rotating machinery, such as compressors for chemical plants, as well as natural phenomena involving exotic, rapidly moving fluids, such as star formation.

The aim of this research project is to model the entropy gain due to viscous dissipation (irreversible conversion of mechanical energy to internal energy due to viscous stress) and irreversible heat transfer over shock waves with different working fluids. With this aim in mind, the following research questions are determined: What is the effect of a fluid's molecular complexity on the thickness of its shock waves at various Mach numbers? What is the effect of a fluid's molecular complexity on the mechanisms of entropy generation within its shock waves at various Mach numbers?

To achieve this, the shock wave will be modeled in a 1-dimensional flow in which the viscous stress and heat transfer are implemented in the continuity, momentum and energy equations. Utilizing numerical integration, the shock profile can be determined along with the entropy production due to both heat transfer and viscous dissipation, allowing for an analysis of the mechanisms which cause energy loss over the shock wave.

II. Method

The analysis performed in this paper aims to describe the mechanisms behind entropy generation in a steady, one-dimensional flow with a normal shock wave, examining mechanisms which occur inside the shock. Calculating the conditions upstream and downstream of such a shock in a control volume is insufficient, as such models fail to encapsulate the mechanisms of entropy generation. Instead, continuous equations of mass, momentum, and energy must be modeled. The general calculation of the continuous shock profile performed in Sections A-C follows the method presented in *The Structure of Shock Waves in the Continuum Theory of Fluids* by Gilbarg and Paolucci [3]. Upon calculation of a continuous shock profile, the entropy generation and shock thickness are calculated following the methods presented in Greitzer's *Internal Flow* [4]. This analysis will be performed for air, water, carbon dioxide, argon, R1234ze(E), and Isobutane in their gaseous states for upstream Mach numbers of 1.04-2.5. The properties of these fluids are gathered from the CoolProp database [5] when not calculated via the methods mentioned below. A link to the GitHub repository with the Python code used to execute the analysis for this paper is found in section IV.

A. Differential forms of equations of mass, momentum and energy

The following set of equations of motion of the steady one-dimensional equations of motion represent the conservation of mass, momentum, and energy, in that order:

$$\frac{d\left(\rho u\right)}{dx} = 0, \tag{1}$$

$$\rho u \frac{du}{dx} = \frac{d\tau}{dx}, \tag{2}$$

$$\rho u \frac{d\left(e + \frac{1}{2}u^2\right)}{dx} = \frac{d\left(\tau u\right)}{dx} - \frac{dq}{dx}. \tag{3}$$

Each of these functions is a function of the position in the single defined spacial dimension, x. The fluid properties in the equations are the density, ρ, the velocity (in x), u, the viscous stress, τ, the specific internal energy, e, and the heat flux in the x direction, q.

Before exploring the above equations further, it is necessary to properly define the fluid properties and outline the simplifying assumptions needed for those definitions. Although the above equations may be implemented for general fluids, this paper restricts the fluids to ideal gases with the following properties outlined for the pressure, internal energy, and gas constant:

$$p = \rho R T, \tag{4}$$

$$e = c_v T, \tag{5}$$

$$R = c_p - c_v, \tag{6}$$

where the constants R, c_p, and c_v are the specific gas constant, and the specific heat constants at constant pressure and volume, respectively. Additionally, we define γ, the ratio of specific heats, to be:

$$\gamma = \frac{c_p}{c_v}. \tag{7}$$

Furthermore, the heat transfer is assumed entirely driven by heat conduction, following Fourier's law of heat conduction:

$$q = -\lambda \frac{dT}{dx}. \tag{8}$$

To complete the description of the fluid properties, the viscous stress, τ, must be defined. Transforming the linear law connecting stress and the rate of deformation in isotropic fluids from three dimensions to one dimension as described in *The Structure of Shock Waves in the Continuum Theory of Fluids* [3], we find that the stress is a function of the pressure, p, the (shear) viscosity, μ_1 and the second (compression) viscosity, μ_2:

$$\tau = -p + \left(2\mu_1 + \mu_2\right)\frac{du}{dx}. \tag{9}$$

Using Stoke's relation,

$$\mu_2 = -\frac{2}{3}\mu_1, \tag{10}$$

it is possible to define a combined viscosity, which can be substituted into Equation 9 to produce a simpler relation for the stress, described in Equation 11:

$$\tau = -p + \mu \frac{du}{dx}, \tag{11}$$

with

$$\mu = 2\mu_1 + \mu_2 = \frac{4}{3}\mu_1. \tag{12}$$

Although the combined viscosity depends only on the shear viscosity, it is noteworthy that both the shear viscosity and the heat conduction are dependent on other fluid properties, such as the temperature. With these relations, the mass, momentum and energy equations may be integrated and combined to create a system of equations which may be solved using numerical integration.

B. Determination of system of equations for numerical integration

The first step in creating a system of equations which may be solved with numerical integration is to take the immediate integrals of Equations 1, 2, and 3, defining the total mass flow, momentum and energy as the constants $\dot{m}$, P, and E, respectively. When substituting the definitions for stress and heat flux, we find:

$$\rho u = \dot{m}, \tag{13}$$

$$\rho u^2 + p - \mu \frac{du}{dx} = P, \tag{14}$$

$$\rho u \left(c_v T + \frac{1}{2}u^2 + \frac{p}{\rho}\right) - \mu u \frac{du}{dx} - \lambda \frac{dT}{dx} = E. \tag{15}$$

With $\dot{m}$, P and E set as constants, we can define the upstream and downstream conditions with the subscript 0 and 1, respectively. In these conditions, the derivatives of temperature and velocity with respect to x are zero:

$$\rho_0 u_0 = \rho_1 u_1 = \dot{m}, \tag{16}$$

$$\dot{m} u_0 + p_0 = \dot{m} u_1 + p_1 = P, \tag{17}$$

$$\rho u_0 \left(c_v T_0 + \frac{1}{2} u_0^2 + \frac{p_0}{\rho_0} \right) = \tag{18}$$
$$= \rho u_1 \left(c_v T_1 + \frac{1}{2} u_1^2 + \frac{p_1}{\rho_1} \right) = E.$$

With these equations, the upstream and/or downstream conditions of the shock which will be calculated by numerical integration may be verified with the above equations. Any pair of upstream and downstream states which satisfy the above equations also satisfy the Rankine-Hugoniot shock conditions.

Equations 13, 14, and 15 can be transformed into a suitable form for numerical integration by substituting the former into the latter two to eliminate ρ, and by utilize the ideal gas law to eliminate p as variables. With further simplification, the system of equations becomes:

$$\mu \frac{du}{dx} = \dot{m} \left(\frac{RT}{u} + u - \frac{P}{\dot{m}} \right), \tag{19}$$

$$\lambda \frac{dT}{dx} = \dot{m} \left(c_v T - \left(u - \frac{P}{\dot{m}} \right)^2 \right) - \frac{E}{\dot{m}} + \frac{P^2}{2\dot{m}^2}. \tag{20}$$

With this system of equations established, and the proper initial conditions are given, it is possible to solve for the unknowns u and T, when as μ, c_v, and λ are all functions of the u, and T. However, finding the correct initial conditions is not trivial. Simply inputting the upstream or downstream conditions will result in constant flow properties, as in Equations 16-18. Additionally, arbitrarily disturbing the upstream or downstream conditions may lead to instability or the inability to traverse the shock, instead returning to the original shock conditions. To overcome this, it is necessary to analyze the normalized direction field of the system of equations.

C. Dimensionless system of equations and determination of initial disturbance

Before determining the stable, nontrivial solution to the given problem, it is useful to first normalize the system of differential equations. To achieve this, we define the dimensionless velocity, ω, dimensionless pressure, ϕ, and dimensionless temperature, θ, as:

$$\omega = \frac{\dot{m} u}{P}, \tag{21}$$

$$\phi = \frac{p}{P}, \tag{22}$$

$$\theta = \frac{m^2 RT}{P^2} = \omega\phi, \tag{23}$$

respectively. Additionally, the dimensionless viscosity and thermal conductivity are defined:

$$\bar{\mu} = \frac{\mu}{\dot{m}}, \tag{24}$$

$$\bar{\lambda} = \frac{\lambda}{c_v \dot{m}}. \tag{25}$$

Finally, another two dimensionless properties, α and δ, which are defined to simplify further notation:

$$\alpha = \frac{2E\dot{m}^2}{P^2} - 1, \tag{26}$$

$$\delta = \frac{1}{2}(\gamma - 1). \tag{27}$$

The system of differential equations may now be written in its dimensionless form:

$$\bar{\mu} \frac{d\omega}{dx} = \omega + \frac{\theta}{\omega} - 1 \equiv M(\omega, \theta), \tag{28}$$

$$\bar{\lambda} \frac{d\theta}{dx} = \theta - \delta \left((1-\omega)^2 + \alpha \right) \equiv L(\omega, \theta). \tag{29}$$

$M(\omega, \theta)$ and $L(\omega, \theta)$ may be used to identify the two states which satisfy the upstream and downstream shock conditions, as trivial solutions to the set of differential equations are found where both $M(\omega, \theta)$ and $L(\omega, \theta)$ are equal to zero. To find these points, the curves $M(\omega, \theta) = 0$ and $L(\omega, \theta) = 0$ are defined as

$$\theta_{M=0} = -\omega^2 + \omega \tag{30}$$

and

$$\theta_{L=0} = \delta \left((1-\omega)^2 + \alpha \right), \tag{31}$$

respectively. Where these parabolas intersect, we find the upstream condition $Z_0 = (\omega_0, \theta_0)$, and the downstream condition $Z_1 = (\omega_1, \theta_1)$. These non-dimensionless values for the upstream and downstream conditions of the shock mirror the Rankine-Hugoniot conditions, and can easily be converted back to their dimensional form. They are entirely dependent on two parameters: δ, which is a fluid constant, and α, which is dependent on the upstream Mach number of the flow:

$$\alpha = \frac{1}{\delta(\delta+1)} \frac{\eta}{(\eta+1)^2}, \tag{32}$$

with

$$\eta = \frac{2\delta + 1}{\delta + 1} M_0^2 - \frac{\delta}{\delta + 1}. \tag{33}$$

With these points outlines, it is now possible to define the solution of the continuous shock wave, or shock profile. The shock profile is a solution $(\omega(x), \theta(x))$ of the system of Equations 28 and 29, with the following properties:

$$(\omega(x), \theta(x)) \to (\omega_0, \theta_0) \text{ as } x \to -\infty, \tag{34}$$

and

$$(\omega(x), \theta(x)) \to (\omega_1, \theta_1) \text{ as } x \to \infty. \tag{35}$$

As x approaches infinity on either side of the shock, it approaches either the upstream or downstream condition. The shock curve and the internal properties of the shock are found to be the integral curve which connects these points in the (ω, θ) plane.

As Z_0 and Z_1 are singular points, and thus trivial solutions, they are insufficient as initial conditions for the shock. Furthermore, it is yet unknown which solutions are stable and meet the conditions outlined in Equations 35 and 35. In order to determine the initial conditions necessary to produce the shock curve via numerical integration, it is useful to analyze the direction field of the

properties (ω, θ), as x increases. An example of such a direction field with the corresponding shock curve is given in Figure 1.

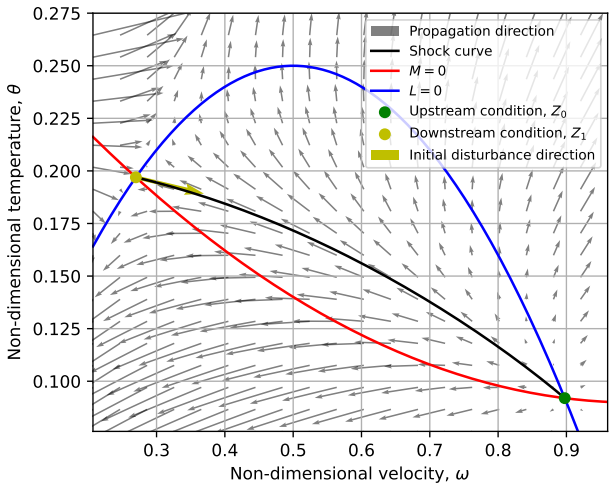

Figure 1: Example non-dimensional shock curve and propagation direction field

There exist a multitude of useful insights which can be extracted from Figure 1. First, we confirm that the upstream and downstream conditions are at the intersections of the $M(\omega, \theta) = 0$ and $L(\omega, \theta) = 0$ lines. The gray arrows display the direction of propagation of the system of linear equations with increasing x. From this information, it becomes evident that Z_0 is an unstable node, from which any disturbance will lead to divergence. The Z_1 node is a saddle point, where disturbances along the shock curve point towards the node, but are still unstable. We also confirm the correctness of the $M(\omega, \theta) = 0$ and $L(\omega, \theta) = 0$ functions, as the change in temperature and velocity, respectively, are zero along those curves. As the velocity must decrease while the temperature increases along the shock, the shock curve must lie between the two curves.

With an unstable node and a saddle point, it is evident that performing numerical integration in the positive x direction will lead to divergence. However, if the calculation is performed from the downstream condition towards the upstream conditions, it is possible to follow the shock curve, given the initial disturbance is correct.

To find the correct initial disturbance, the integral curves which approach Z_1 as $x \to +\infty$ must be found. One of these will determine the slope $(\frac{d\theta}{d\omega})$ of the initial disturbance. To find the slope of the shock curve at Z_1, the characteristic equation of the saddle point may be used:

$$0 = \left| \begin{matrix} \frac{M_\omega}{\bar{\mu}} - \zeta & \frac{M_\theta}{\bar{\mu}} \\ \frac{L_\omega}{\bar{\lambda}} & \frac{L_\theta}{\bar{\lambda}} - \zeta \end{matrix} \right|_{Z=Z_1}, \tag{36}$$

where the subscripts ω, θ represent partial differentiation and ζ represents the eigenvalues of the characteristic equation. The partial derivatives of M and L are given as

$$M_\omega = 1 - \frac{\theta}{\omega^2}, \tag{37}$$

$$M_\theta = \frac{1}{\omega}, \tag{38}$$

$$L_\omega = 2\delta(1 - \omega), \tag{39}$$

$$L_\theta = 1. \tag{40}$$

With this established, the eigenvector corresponding to the negative eigenvalue, ζ, of Equation 36 can be determined. This eigenvector is displayed as the initial disturbance direction in Figure 1. With the initial disturbance calculated, it is possible to follow the shock curve while incrementally decreasing x. The shock curve is found by numerically integrating the following equation until Z_0 is approached sufficiently:

$$\frac{d\theta}{d\omega} = \frac{\bar{\mu} L(\omega, \theta)}{\bar{\lambda} M(\omega, \theta)}. \tag{41}$$

The result of this integration provides both the shock curve as a set of elements $(\omega(x), \theta(x))$ as a function of x. An example shock curve is displayed as the black curve connecting Z_0 and Z_1 in Figure 1. Finally, the non-dimensional variables can be reverted to their dimensioned form, if necessary, concluding the construction of the shock as presented by Gilbarg and Paolucci [3].

D. Determination of shock thickness and mechanisms of entropy generation

With a given shock curve as calculated in Sections A-C, it is possible to determine the shock's thickness and entropy generation mechanisms. the shock thickness is determined by the difference in velocity upstream and downstream of the shock, and the largest velocity gradient along the shock:

$$t = \frac{u_0 - u_1}{\left| \frac{du}{dx} \right|_{max}}. \tag{42}$$

It is also possible to analyze the shock thickness in terms of mean free path:

$$t_{mfp} = \frac{u_0 - u_1}{\left| \frac{du}{dx} \right|_{max} \ell_{mfp}}, \tag{43}$$

where the mean free path, ℓ_{mfp} is given by the Maxwell mean free path of a molecule in the upstream condition:

$$\ell_{mfp} = \frac{\mu_0}{\rho_0} \sqrt{\frac{\pi}{2RT_0}}. \tag{44}$$

Finally, the entropy generation can be analyzed. The entropy generation over a shock can be described by two effects: the entropy generation due to viscous forces and the entropy generation due to heat dissipation. Each of these can be determined separately and compared:

$$\frac{ds_{\text{visc}}}{dx} = \frac{\mu}{T\dot{m}} \left(\frac{du}{dx} \right)^2, \tag{45}$$

$$\frac{ds_{\text{heat}}}{dx} = \frac{\lambda}{T^2\dot{m}} \left(\frac{dT}{dx} \right)^2. \tag{46}$$

By numerically integrating over the shock curve, it is possible to extract the total entropy generated over the shock, the types of entropy generation and how the entropy is generated along the shock profile.

III. Results and discussion

The methods described in the previous chapter were applied to argon, air, water, carbon dioxide, isobutane and R1234ze(E) in their gaseous states over a range of Mach numbers. First, individual shocks are analyzed, ensuring the correct execution of the method. With this analysis, the structure of the shock waves is also discussed. Following this, the shock thickness and methods of entropy generation are compared between the different fluids at various Mach numbers. The mechanisms behind the differences are also discussed.

A. Analysis of single shocks

Before answering the research questions, it is pertinent to analyze individual shocks to determine their structure and verify the accuracy of the code. For this purpose, the shock curve of air with an upstream Mach number of 2.5, upstream temperature of 300°K and upstream pressure of 100000 Pa. First, the velocity, temperature, and pressure profiles over the shock are analyzed and validated. These curves are presented in figures 2, 3, and 4, respectively. Then, the entropy generation and thickness are discussed.

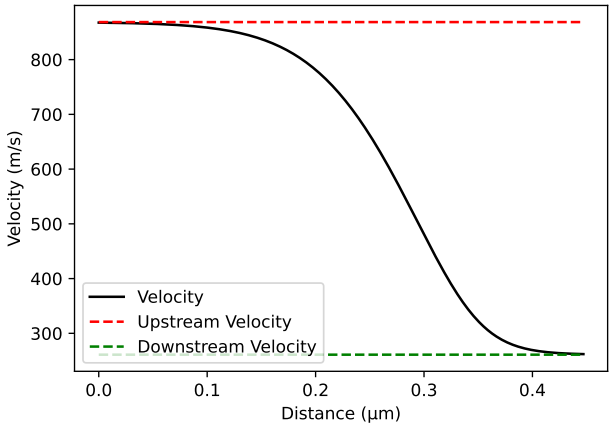

Figure 2: Calculated velocity profile over shock in air at Mach 2.5

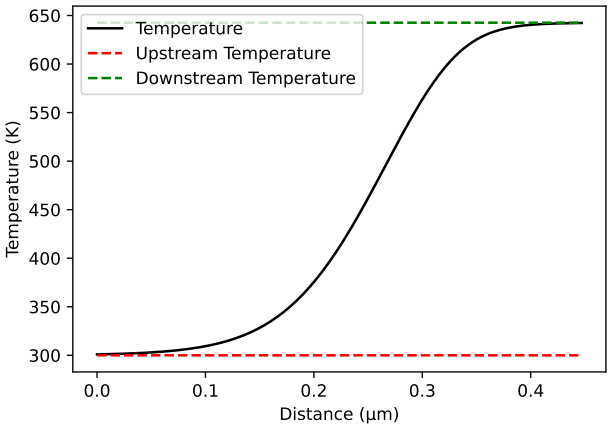

Figure 3: Calculated temperature profile over shock in air at Mach 2.5

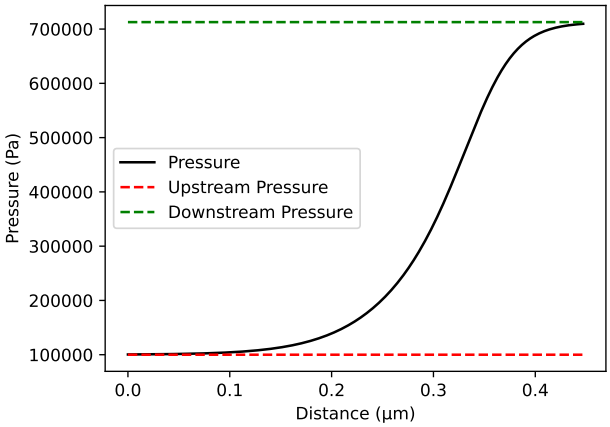

Figure 4: Calculated pressure profile over shock in air at Mach 2.5

What is notable about the method used is that there is a degree of validation which is inherent to the model, as the upstream and downstream velocities, temperatures and pressures are known independently via the Rankine-Hugoniot condition. These values are displayed in figures 2-4. Since the numerical integration scheme is upwind, it is possible to compare the upstream conditions of the model and the input to confirm the correct end result. For all shocks computed, this is the case. However, this does not validate the correctness of the shock profile itself, which is entirely dependent on the model. The correctness of the model has thus been verified with other implementations, as presented by Greitzer [4] and Teeple [6]. The shock profile is best described by analyzing the velocity, temperature and pressure simultaneously, as shown in figure 5.

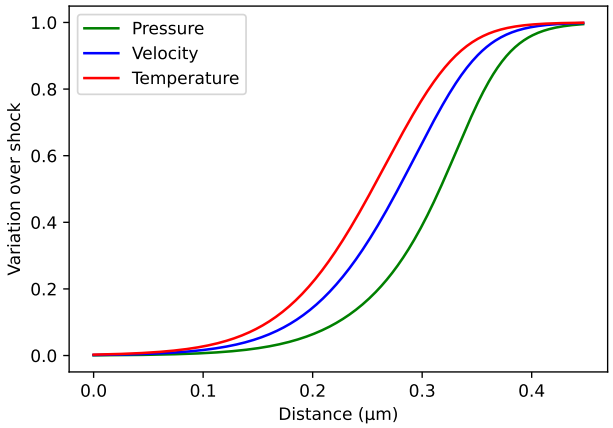

Figure 5: Variation of velocity, temperature and pressure over Mach 2.5 shock in air

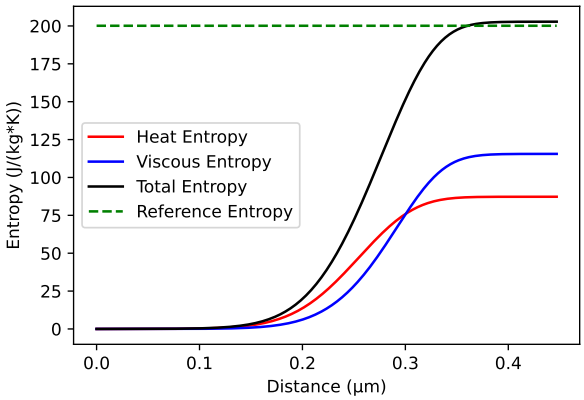

Figure 6: Entropy generation over Mach 2.5 shockwave in air, compared to reference calculation

Figure 5 displays the change in velocity, temperature and pressure over a shock in air at Mach 2.5. The abscissa represents the distance from the upstream condition, the ordinate shows the relative change in the three parameters, where 0 denotes the upstream condition and 1 denotes the downstream condition.

As shown, the temperature change drives the creation of the shock, as it rises first. This is followed by a drop in velocity, then a rise in pressure. This is consistent among all calculated shocks and Mach numbers. Whereas the temperature leads the other two by nearly the same distance for all Mach numbers, the temperature tends to lead less for increasing molecular complexity.

The initial change in these parameters is relatively gradual, steadily increasing until the inflection point. As the shock reaches the downstream condition, the higher temperature enables a 'faster' interaction between particles, speeding up the shock process. This is seen as a sharper curve near the top of figure 5. This effect becomes more pronounced as the Mach number increases, as the temperature difference over the shock increases. By the definition of shock thickness given in equation 42, we find the shock thickness to be 0.156 μm, or 0.391 mean free paths. The entropy generation over the same shock is presented in figure 6.

The two types of entropy generation over the shockwave are highly linked to the temperature and velocity changes. This effect is displayed in figure 7, which compares the types of entropy generation to the three fluid properties discussed above.

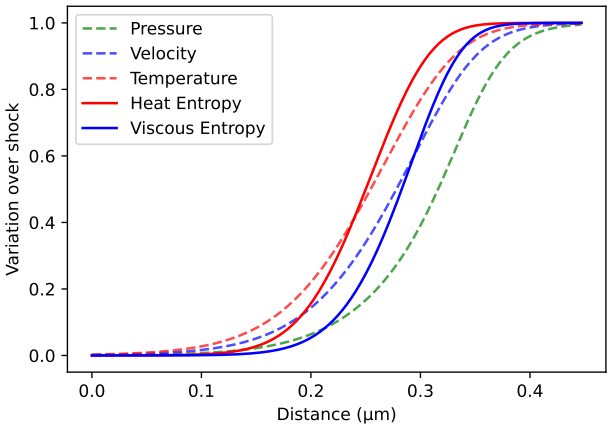

Figure 7: Normalized entropy generation contributions due to heat and viscous effects compared to shock velocity, temperature and pressure profiles

In figure 7, each process of entropy generation is normalized on a scale ranging from 0 for the upstream value to 1 for its downstream value. The same transformation is performed on the velocity, temperature and pressure profiles. This is done to highlight the link between the entropy generation types and the three fluid properties. It is evident that the change in temperature drives the entropy generated due to heat conduction, whereas the velocity change contributes to the entropy change due to viscous dissipation. Due to this, the entropy generated due to heat conduction precedes the entropy due to viscous dissipation.

The total entropy generated is verified by comparing the final entropy generated to the discontinuous entropy jump given in equation 47 [7].

$$\Delta s = c_v \log\left(\frac{T_0}{T_1}\left(\frac{u_1}{u_0}\right)^{\gamma-1}\right) \tag{47}$$

The accuracy of the entropy model generally decreases with molecular complexity. Argon exhibits the smallest entropy discrepancy over the range of Mach 1.1-2.5, with the largest difference in entropy lying under 0.28%. The discrepancy between the continuous and discontinuous models remains below 1.35% for air, 6.09% for water, 4.00% for carbon dioxide, 3.74% for R1234ze(E), and 4.02% for Isobutane. These differences are likely due to the change in viscosity and thermal conductivity over the shock causing slight variations in the entropy calculations.

B. Comparison of shock thickness of multiple fluids

With the accuracy of the model verified for single shocks, it is possible to compare the reaction of different fluids to shocks. For these simulations, the upstream fluid conditions were set at 300°K and 100000 Pa. To ensure that each fluid remained in its gaseous state during the simulation, the initial temperature of water was set to 400°K. First, figure 8 shows the relation between shock thickness and Mach number for fluids of differing molecular complexity.

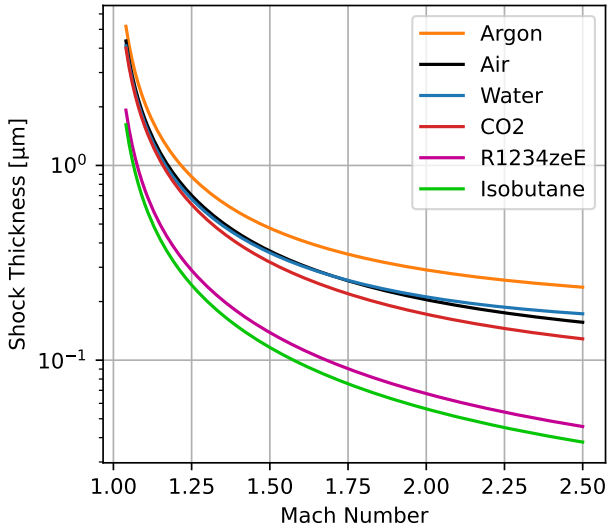

Figure 8: Shock thickness of multiple fluids at multiple Mach numbers

As the molecular complexity increases, the shock thickness tends to decrease. Argon, being monoatomic, is the simplest molecule, and displays the thickest shock. R1234ze(E) and Isobutane are the most complex molecules in this study, and have shocks which are an order of magnitude thinner than argon, air and water. The larger number of degrees of freedom in these fluids contributes to faster interaction and shock propagation.

Additionally, the shock thickness decreases with shock intensity. As the upstream Mach number increases, the temperature and pressure difference over the shock become greater, likely leading to a more abrupt shock. This effect is slightly less pronounced for water, likely due to the higher initial temperature required to ensure the water is in its gaseous state. This change generally increases the shock thickness compared to the other fluids, explaining its large shock thickness compared to the trend, and compared to carbon dioxide.

To compensate for molecular complexity, it is possible to normalize the shock thicknesses to the mean free path of the molecules. This is presented in figure 9.

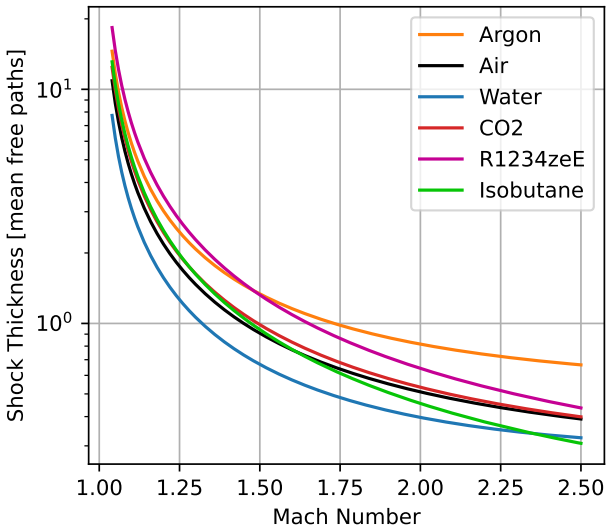

Figure 9: Mean free path normalized shock thickness of multiple fluids at multiple Mach numbers

When normalized to the mean free path, the shock thickness remains highly dependent on the Mach number, but the correlation between molecular complexity and shock thickness disappears. However, for more complex molecules, such as Isobutane or R1234ze(E), the shock thickness decreases at a faster rate than for simpler molecules.

C. Comparison of shock entropy generation for multiple fluids

The types of entropy generation vary greatly for different fluids and different shock strengths. The fluid properties highly affect whether the majority of entropy generation occurs due to heat conduction or due to viscous dissipation. Figure 10 compares the ratio of the types of entropy generation for multiple shocks. As the molecular complexity increases, the temperature difference over the shock decreases. This effect is driven by the ratio of specific heats, γ, which is a key component in determining the temperature and velocity change for a given shock. Molecules with smaller ratios of specific heat have more 'degrees of freedom', which each can absorb some of the heat energy, decreasing the temperature gain over the shock. Conversely, the velocity change over shocks in fluids with large molecular complexity is larger than

for lower molecular complexity. The reduction in temperature difference reduces the entropy generation due to heat conduction, as less heat is conducted across the shock. The greater velocity difference is accompanied by a greater increase in density over the shockwave, which leads to a greater proportion of entropy produced by viscous effects.

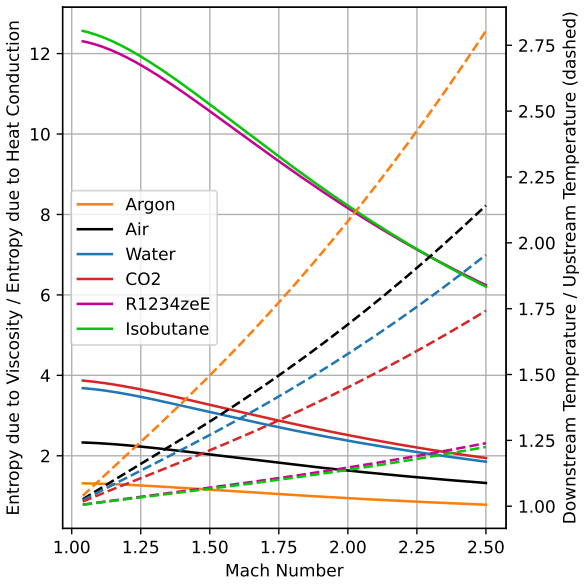

Figure 10: Ratio of entropy generation due to viscous dissipation to entropy generation due to heat conduction and relation to temperature change over shocks for multiple fluids at multiple Mach numbers

Figure 10 clearly shows these trends, as R1234ze(E) and isobutane have the largest proportion of entropy production due to viscous effects, while displaying low change in temperature over shocks. Argon shows the greatest temperature difference over shocks, and the largest proportion of entropy generated due to heat conduction. It seems that the ratio of entropy production types is loosely proportional to $\frac{1}{\gamma-1}$, which is also the ratio between temperature change and density change in an adiabatic system.

Additionally, as the Mach number increases, the proportion of entropy generated due to heat conduction increases for all fluids. This is quite an interesting result, as the entropy produced by heat conduction is proportional to $(\frac{1}{T}\frac{dT}{dx})^2$, whereas the entropy produced by viscous effects is proportional to $\frac{1}{T}(\frac{du}{dx})^2$. It is evident that the temperature gradient change with increasing Mach number drives the ratio of entropy production methods more than the temperature difference and the velocity gradient. However, both the entropy generated by viscous effects and heat conduction increase drastically with increasing Mach number.

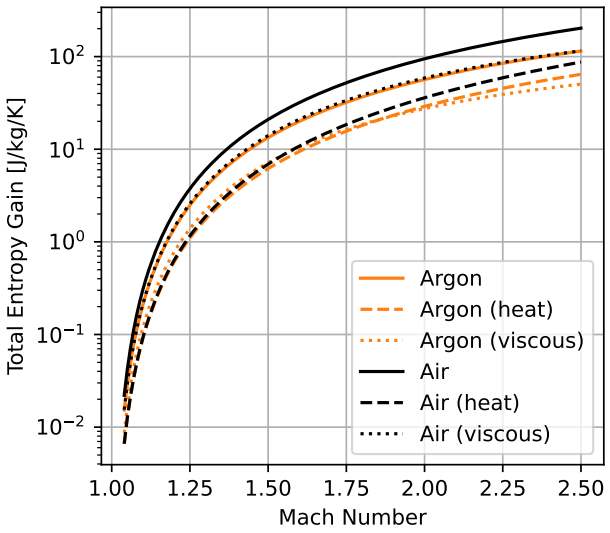

Figure 11: Entropy production over shocks in argon and air at multiple Mach numbers

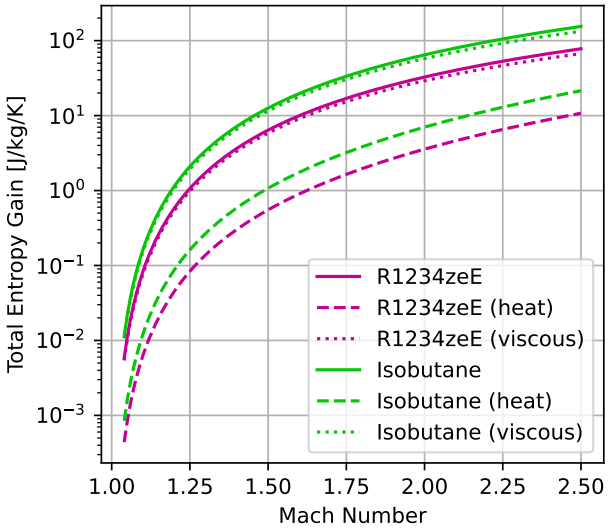

Figure 12: Entropy production over shocks in R1234ze(E) and Isobutane at multiple Mach numbers

Figures 11 and 12 show the total entropy gain over shocks for the molecularly simplest and most complex fluids, respectively, for a range of Mach numbers. The entropy generated by heat conduction and viscous effects are also shown. The entropy generated by both effects increases significantly with increasing Mach number. The figures also highlight the dominance of viscous effects in entropy generation for complex molecules. Conversely, in argon and air both conduction and viscous dissipation contribute significantly to the entropy gain. Note that the slope of the entropy gain steadily increases with increasing Mach number, which is not visible in the figure due to the logarithmic y-axis.

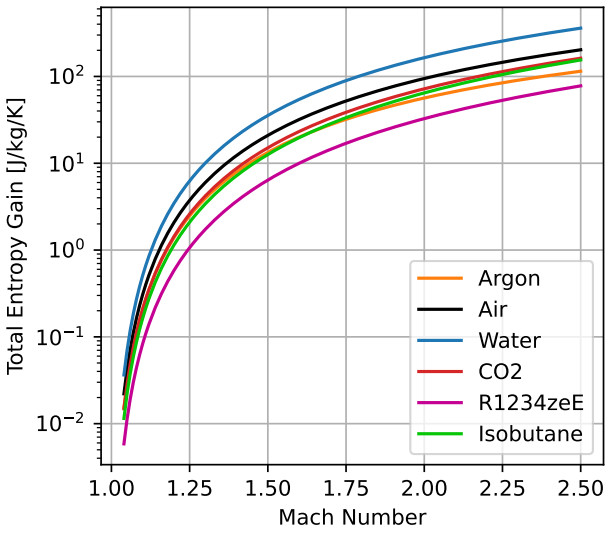

Figure 13: Total entropy production over shocks in multiple fluids at multiple Mach numbers

Figure 13 shows the total entropy gain over shocks of all fluids presented in this analysis. With the fluids at hand, there is no clear correlation between the molecular complexity and the total entropy generation, though the entropy generation does vary for each fluid. Note that the increased initial temperature of water increases the entropy gain relative to the others. Again, increasing the Mach number increases the entropy gain over the shock significantly. It is recommended to further research the impact of molecular complexity on the total entropy gain, as there may be some correlation which was not found with the fluids analyzed in this paper.

IV. Conclusion and Recommendations

The aim of this paper was to determine the effect of molecular complexity on the internal structure of shock waves. In particular, the shock thickness and the mechanisms of entropy generation were studied.

The equations governing the conservation of mass, momentum and energy in a 1-dimensional flow were applied for this purpose. These equations were modified to allow for numerical integration over a shock to determine its internal properties, simulating a continuous shock. With this model, the internal and downstream conditions could be determined for arbitrary gaseous fluids with arbitrary upstream conditions. These conditions in turn allowed for the determination of the shock thickness and entropy generation methods over the shock. These parameters were compared for varying fluids and Mach numbers.

The model reveals various details pertaining to the internal shock structure. Within a shock, sharp increases in temperature precede increases in density and then pressure. This effect remains constant for increasing Mach number, but becomes less pronounced with increasing molecular complexity.

The entropy rise over a shock is driven by two mechanisms: heat conduction over the shock and viscous dissipation within it. The entropy rise due to heat conduction is primarily affected by the increase in temperature over the shock, and this entropy rise occurs proportionally to the square of the rate of temperature change within the shock. This mechanism slightly precedes the entropy rise due to viscous dissipation, which is driven by the square of the rate of change in density over the shock. This falls in line with the rate of change in velocity, which is slightly delayed from the temperature rise.

The proportion of entropy gain due to viscous effects rises with increasing molecular complexity, as the temperature difference over the shock is lower for fluids with molecules with more degrees of freedom. As the Mach number rises, the proportion of entropy gained from viscous effects also decreases. However, the total entropy due to both effects increases with Mach number, as the shock intensity increases. With the fluids analyzed in this study, no correlation between total entropy generation and molecular complexity was found. It is recommended to extend this study to more fluids with varying molecular complexity to analyze this further.

The shock thickness decreases with both increasing molecular complexity and increasing upstream Mach number. The former effect is likely due to the shorter mean free path of the complex molecules. There is no definitive correlation between molecular complexity and shock thickness when measured in terms of mean free path.

With these insights, it is possible to analyze the losses in rotating machinery more optimally. This could allow for the design process behind rotating machinery with complex molecules to take the mechanisms behind the different types of entropy gain – and thus fluid-dynamic loss – into account. It is recommended to further investigate these effects in the context of the optimization of rotating machinery.

It is also recommended to expand the model to account for more gases. First, the CoolProp library offers limited data on thermal conductivity and viscosity for many fluids, limiting the range of fluids which may be applied. It is recommended to broaden this study to more fluids through use of different databases or models to determine properties. This would enable a more comprehensive analysis into the research questions posed in this paper.

Finally, it is recommended to investigate the effects of the use of the ideal gas law in this study. Implementing more accurate models for the equation of state of fluids, such as the van der Waals equation of state, may reveal inaccuracies of the model discussed in this report for some fluids. This would enable the investigation of the internal conditions of shocks in non-ideal gases as well.

References

[1] Astolfi, M., Baresi, M., Buijtenen, J., Casella, F., Colonna, P., David, P., Öhman, H., Sánchez, D., and

Wieland, C., "Thermal Energy Harvesting: The Path to Tapping into a Large CO2-free European Power Source," *Knowledge Center on Organic Rankine Cycle technology*, 2022.

[2] Tosto, F., *Modeling and characterization of non-ideal compressible flows in unconventional turbines*, Ph.D. thesis, Delft University of Technology, 2023.

[3] Gilbarg, D. and Paolucci, D., "The Structure of Shock Waves in the Continuum Theory of Fluids," *Indiana University Mathematics Journal*, Vol. 2, 1953, pp. 617–642.

[4] Greitzer, E. M., Tan, C. S., and Graf, M. B., *Internal flow : concepts and applications*, Cambridge University Press, 2004.

[5] Bell, I. H., Wronski, J., Quoilin, S., and Lemort, V., "Pure and Pseudo-pure Fluid Thermophysical Property Evaluation and the Open-Source Thermophysical Property Library CoolProp," *Industrial & Engineering Chemistry Research*, Vol. 53, No. 6, 2014, pp. 2498–2508.

[6] Teeple, B., "An Investigation into Local Entropy Generation in Shock Waves," Tech. rep., Massachusetts Institute of Technology, 1995.

[7] Anderson, J. D. and Cadou, C., *Fundamentals of aerodynamics*, McGraw-Hill, 7th ed., 2024.

Appendix A

The program used to perform the analysis of this paper is found here: `https://github.com/sbcox/TUDelft_BSc_Honors_Project`